ON THE INFLUENCE OF MICROSTRUCTURE UPON CRACK PROPAGATION MECHANISM AND FRACTURE TOUGHNESS

A. Halim*, D.-Z. Sun** and W. Dahl*

Using a combination of numerical and experimental methods two different types of low strength steels Fe 510 have been investigated for describing the influence of microstructure on crack propagation mechanism and fracture toughness. The microstructure parameters have been determined by means of quantitative metallographic techniques.

INTRODUCTION

Today one of the most important aims in technical research on structural materials is to investigate the influence of microstructure on crack propagation mechanism and fracture toughness. During plastic deformation in ductile metals, damage is mainly described by nucleation (a), growth (b) and coalescence (c) of voids (1,2,3). For ductile fracture the latter stages, void growth and coalescence, are more important. McClintock (4,5) and Rice and Tracey (6) have shown that void growth strongly depends upon the rate of specimen extension and the state of stress, especially upon the ratio of mean stress to effective flow stress.
The coalescence of the first voids ahead of the crack tip can be defined as the onset of stable crack growth, indicated by J_i or δ_i, respectively.

* Institute for Ferrous Metallurgy, Technical University Aachen, D-5100 Aachen, FRG
** Fraunhofer-Institut für Werkstoffmechanik, Wöhlerstr. 11, D-7800 Freiburg, FRG

Definition of stress and strain state parameters

Three parameters of stress and strain state are used throughout; effective flow stress σ_v, mean stress σ_m and effective plastic strain ε_v^p, defined as follows in terms of the principal stresses σ_1, σ_2 and σ_3, and the increments of principal plastic strains $d\varepsilon_1^p$, $d\varepsilon_2^p$ and $d\varepsilon_3^p$.

$$\sigma_v = \sqrt{\frac{1}{2}\left[(\sigma_1-\sigma_2)^2 + (\sigma_2-\sigma_3)^2 + (\sigma_3-\sigma_1)^2\right]} \qquad (1)$$

$$\sigma_m = \frac{\sigma_1+\sigma_2+\sigma_3}{3} \qquad (2)$$

$$d\varepsilon_v^p = \sqrt{\frac{2}{9}\left[(d\varepsilon_1^p-d\varepsilon_2^p)^2 + (d\varepsilon_2^p-d\varepsilon_3^p)^2 + (d\varepsilon_3^p-d\varepsilon_1^p)^2\right]} \qquad (3)$$

The two stress parameters can be combined into a single non-dimensional parameter σ_m/σ_v which characterizes a stress state and is a measure of its "triaxiality". In a uniaxial tension test σ_m/σ_v is 0.3, before necking. According to Bridgman (7), σ_m/σ_v and ε_v^p in the central region of the specimen, where failure initiates, can be described as:

$$\frac{\sigma_m}{\sigma_v} = \frac{1}{3} + \ln\left(\frac{d}{4\rho} + 1\right) \qquad (4)$$

$$\varepsilon_v^p = 2 \cdot \ln\left(\frac{d_o}{d}\right) \qquad (5)$$

where d_o = original specimen diameter
d = actual specimen diameter
ρ = actual notch radius

The same non-dimensional stress state parameter (σ_m/σ_v) has been used by several authors (8,9,10) to present ductile failure loci in which the strain to initiate failure is presented as a function of the state of stress (σ_m/σ_v).
In this work the influence of stress state upon the plastic strain at failure is evaluated on axisymmetric, circumferentially notched tensile specimens for six different notch radii ρ_o (ρ_o = 0.25; 0.5; 1; 2; 4 mm and $\rho_o = \infty$).

Finite element (FE) analysis (11,12) have shown that both the effective plastic strain and the severity of the stress state in the centre of the specimen cannot be estimated precisely by Bridgman's formula in the case of sharp notches. When the notch

radius becomes larger the agreement between both values becomes better. Within the scope of this work, these critical strain and stress values according to Bridgman will be compared with the results of FE-calculations.
The calculations have been carried out on specimens with sharp notches (ρ_0 = 1 mm and 0.25 mm) with the eight-node element mesh (figure 1); a reduced integration scheme (2x2) has been adopted in order to avoid the violation of incompressibility conditions. The deformation of the mesh geometry has been taken into account using the so called "updated lagrange" to modify the coordinates for each load step. One fourth of the specimen was sufficient to idealize the FE-model (see also figure 1).

RESULTS

Experimental results

The tensile and fracture tests have been performed on two types of steel Fe 510, one of them with a reduced carbon content and higher purity; in comparison to the standard version (0.0195%) the sulphur content of the pearlite reduced quality was determined to 0.002%. Finally, to assure a similar strength level, it contained some Vanadium and Niobium. For either steels, the microstructure is characterized by ferrite with bands of pearlite, being less pronounced in the pearlite reduced quality. Due to the addition of the microalloying elements, the mean ferrite grain size for the pearlite-reduced steel is smaller than for the other material, the values being 5.5 µm and 15.0 µm (13).
Based on the lower sulphur content, the mean distance of MnS-inclusions S has been determined to 110.3 µm in case of pearlite-reduced quality, in contrast to 42.2 µm for the standard version. These values and the results of the tensile tests on notched and unnotched specimens are listed in table 1.

Numerical results

The results of the tensile tests are presented in figure 2a (Fe 510) und 2b (pearlite-reduced). In the figure above the load is plotted as a function of the reduction of the specimen diameter for ρ_0 = 0.25 mm, below for 1 mm. The dashed lines result from experiment, the solid ones are calculated. The comparison reveals a quite good agreement, but as soon as ductile damage starts, the difference between the curves increases. The main problem is to detect the point of failure initiation; FE-calculations do not indicate this phenomenon, e.g. after some work hardening a sharp drop of load, suggesting a sudden reduction in cross section area. Nevertheless, the results of this work suggest that initiation might correspond to a first deviation between experiment and calculated curve, beyond maximum load. In figure 2 these points are marked with arrows and indices i.
Figures 3a and 3b show the effective plastic strain ε_v^p as a function of the distance from the specimen centre, with the applied load as parameter. The values of ε_v^p increase from the centre of

the specimen up to the notch with the maximum value at the notch root. The corresponding values according to Bridgman (eq. (5)) are constant (dashed lines).

Corresponding to figure 3, figures 4a and 4b show the stress state parameter. The ε_v^p- and the σ_m/σ_v-values for initiation of fracture are again marked with arrows. It can be seen, that, for ρ_o = 0.25 mm, the maximum values were found near the notch root, for ρ_o = 1 mm, these maximum values disappear more and more with increasing plasticity. As simple failure initiation condition it can be assumed, that ε_v^p must reach a critical value at the root of the notch; as figures 3 and 4 indicate, the corresponding value for the stress state (σ_m/σ_v) shows a minimum. On the other hand - from a microscopic and physical point of view -, failure can not depend upon the stress and strain at a certain point, but over a characteristic length or volume, related to the microstructure.

Thus, a modified failure initiation condition is necessary; ε_v^p must exceed a critical value over a certain critical distance l_c, and this distance l_c, known as the material size parameter, is not necessarily located immediately ahead of the notch but may be found in the centre of the sample. So, for predicting failure initiation, both the σ_m/σ_v- and ε_v^p-values have to be taken into account.

In this work the microstructural critical distance l_c has been determined by light microscope. Figure 5 shows the photo of two notched specimens with ρ_o = 0.25 mm (above) and ρ_o = 1 mm (below). The tensile tests had been stopped immediately beyond maximum load and the specimens afterwards have been examined metallographically; therefore they had been cut in the centre in axial direction. One can see very well, that for ρ_o = 0.25 mm failure initiates near the tip of the notch, while, if ρ_o is large enough initiation begins in the centre of the specimen. The critical distance l_c was determined to 0.52 mm (see also figure 5). The values for σ_m/σ_v and ε_v^p, corresponding to initiation, are listed in table 1.

Figure 6 shows the effective plastic strain as a function of stress state. Obviously there is a strong dependency for both steels. The hollow symbols result from Bridgman's equations (eqs. (4) and (5)). Both FE-calculation and Bridgman's formula show a strong decrease of the effective plastic strain with increasing triaxiality, until, at about $\sigma_m/\sigma_v \sim 1$, the curves approach a rather constant level of about ε_i = 0.14 and 0.58, respectively. As it can be seen from the diagram, two geometries have been compared; while, according to Bridgman, the smaller notch radii show the higher values σ_m/σ_v, the FE calculations seem to indicate the opposite. All these curves can be approached very well by an exponential function, viz:

$$\varepsilon_f^* = \alpha \cdot \exp(-\beta \cdot \sigma_m/\sigma_v) + \varepsilon_i \qquad (6)$$

The values for β were found between 5 and 16, that means considerably above the theoretical value 1.5 (8).

Correlation between microstructure and fracture toughness

The fracture mechanics values have been determined according to ASTM E813 (14) on CT specimens with a/W = 0.6 and 20% side grooves. At the onset of crack extension the J_i-values have been evaluated using the direct current potential drop (DCPD)-method. Figure 7 shows the R-curves for the steels examined, resulting from fracture mechanics tests. Due to the reduced carbon content and to microalloying, the pearlite-reduced quality shows by far the better crack extension behaviour. The J_i-values are marked by arrows.

In order to describe the relationship between microstructure and ductile fracture, the critical strain criterion was applied inside this work. There are different models to describe the strain distribution at the crack tip, e.g. McMeeking (15), Rice and Johnson (16) and the HRR-field (17). In (10) the strain distribution for each of these models has been discussed and compared quantitatively. To determine the effective plastic strain, the HRR-solution was used:

$$\varepsilon_v^p = \alpha \cdot \varepsilon_y \cdot \left(\frac{J}{\alpha \cdot \sigma_y \cdot \varepsilon_y \cdot I_N \cdot r}\right)^{N/(N+1)} \cdot \hat{\varepsilon}^p(\Theta,N) \qquad (7)$$

with

α, N = Ramberg-Osgood constants
σ_y = yield stress
ε^y = σ_y/E is the yield strain
E^y = Young's modulus
I_N, Θ = dimensionless constants, HRR-field function

$$\hat{\varepsilon}^p(\Theta,N) = \left[\hat{\sigma}_e(\Theta,N)\right]^N$$

and for initiation

$$J = J_i \qquad \varepsilon_v^p = \varepsilon_i$$

$$r = l_c$$

In table 1 the calculated values for l_c are listed, beeing about three times the magnitude of the mean distance of MnS-inclusions. In any case, they are considerably smaller than those determined by light microscope.

SUMMARY

Two types of steel Fe 510 have been investigated in order to find a correlation between microstructure and fracture toughness.
Up to the onset of instability the global material behaviour can be described very well by finite element analyses using the so called "updated lagrange".
It could also be shown that the Bridgman formula cannot describe

the strain and stress distribution corresponding to initiation, if the notch radii of the specimen are small.
When trying to correlate between microstructure and fracture toughness, the following requirements must be fulfilled:
- a proper criterion for ductile fracture must be chosen
- stress or strain distribution ahead of the crack tip must be known
- a good conception for determining the microstructural critical distance l_c is necessary. Inside this work, the values for l_c proved to be about three times the mean distance of MnS-inclusions. The values observed by light microscope proved to be higher.

ACKNOWLEDGEMENT

The authors gratefully acknowledge the financial support of the DFG (Deutsche Forschungsgemeinschaft).

REFERENCES

(1) McClintock, F.A., Ductility, A.S.M., 1968, p 255
(2) Thomason, P.F., J. Inst. Metals, 98, 1968, p 360
(3) Brown, L.M. and Embury, J.D., Proc. 3rd Int. Conf. Strengths of Met. and Alloys, Cambridge, U.K., 1973, p 164
(4) McClintock, F.A., J. of appl. Mech., June 1968, pp 363/71
(5) McClintock, F.A., Kaplan, S.M. and Berg, C.A., Int. J. Fract. Mech. 2, 1966, pp 614/27
(6) Rice, J.R. and Tracey, D.M., J. of Mech. and Phys. Solids, 17, 1969, pp 201/17
(7) Bridgman, P.W., Studies in large flow and fracture, New York 1952
(8) Hancock, J.W. and Mackenzie, A.C., J. Mech. Phys. Sol. 24, 1976, p 147
(9) Mackenzie, A.C., Hancock, J.W. and Brown, D.K., Engng. Fract. Mech., 9, 1976, p 167
(10) Sun, D.-Z., Halim, A. and Dahl, W., 19. Sitzung AK Bruchvorgänge der DVM, Freiburg, 1987, pp 303/13
(11) Hancock, J.W. and Brown, D.K., J. Mech. Phys. Solids 31, 1983, pp 1/24
(12) Beremin, F.M., Journal de Mecanique appliqueê, 4, 1980, pp 307/25
(13) Halim, A. Diploma Thesis, RWTH Aachen, 1983
(14) ASTM 813-81, Annual Book of ASTM Standards, Philadelphia, American Society for Testing Materials, 1983
(15) McMeeking, R.M., J. Mech. Phys. Sol. 25, 1977, pp 357/81
(16) Rice, J.R. and Johnson, M.A., Inelastic Behaviour of Solids, Ed. Kanninen et al., McGraw Hill, New York, 1970, pp 641/72
(17) Shih, C.F., Tables of Hutchinson-Rice-Rosengren Singular Field Quantities, Brown University, MRL E-147, 1983

steel	experiment σ_m/σ_v | ε_y^p	FE-calculation σ_m/σ_v | ε_y^p	N -	σ_y [MPa]	S [µm]	cal. l_c [µm]
Fe 510	ρ_o=0.25mm 2.21 | 0.11 ρ_o=1.0mm 0.91 | 0.24	ρ_o=0.25mm 1.0 | 0.11 ρ_o=1.0mm 1.4 | 0.12	4.55	330	42.2	135
Fe 510 pearl.red.	ρ_o=0.25mm 1.55 | 0.53 ρ_o=1.0mm 1.16 | 0.55	ρ_o=0.25 0.88 | 0.48 ρ_o=1.0mm 1.55 | 0.46	5.0	383	110.3	284

Table 1 - tensile tests, quantitative metallographic results and calculated l_c

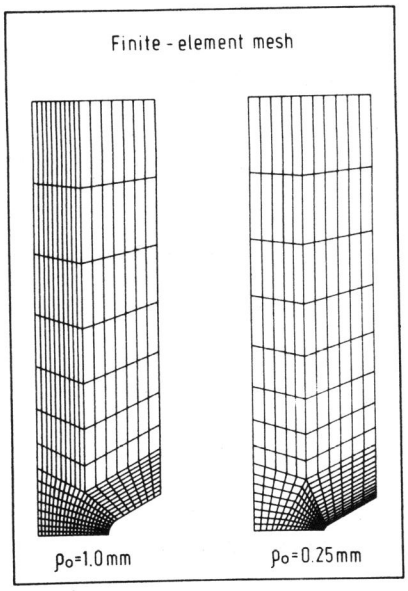

Figure 1 finite element mesh

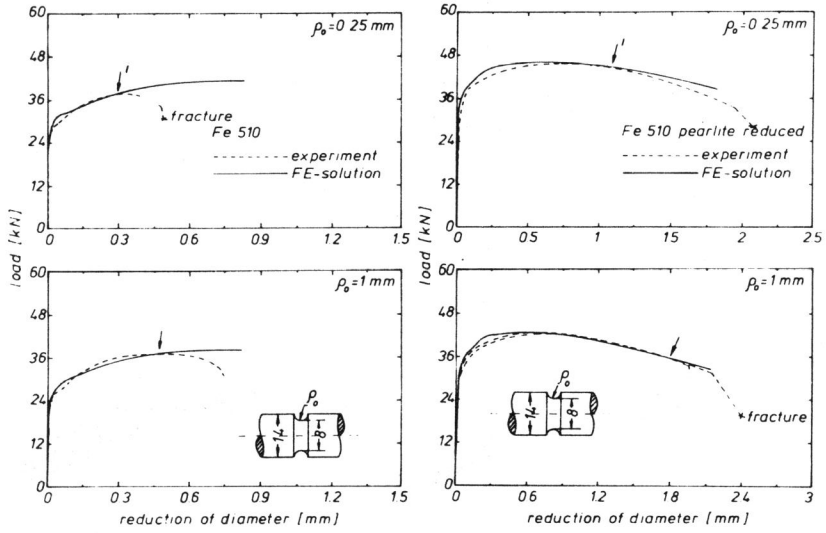

Figure 2 tensile tests, experiments and calculated

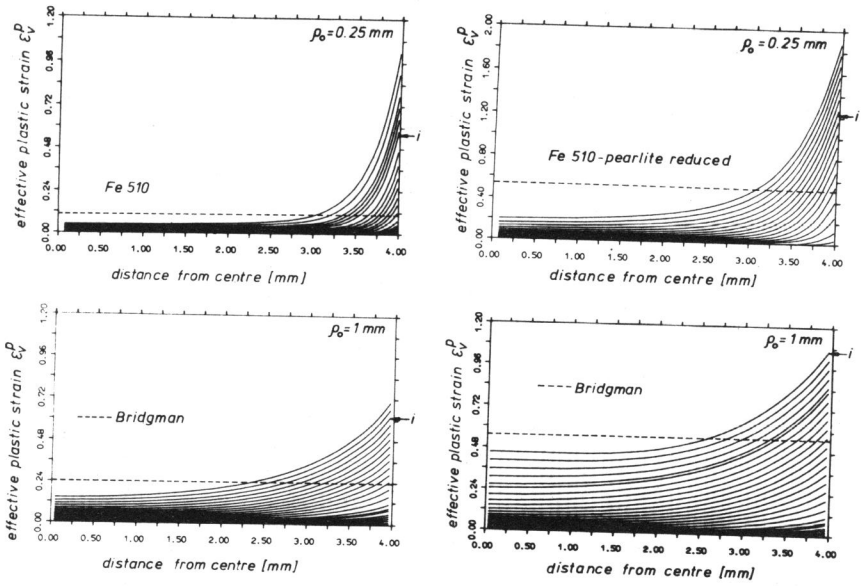

Figure 3 effective plastic strain, calculated

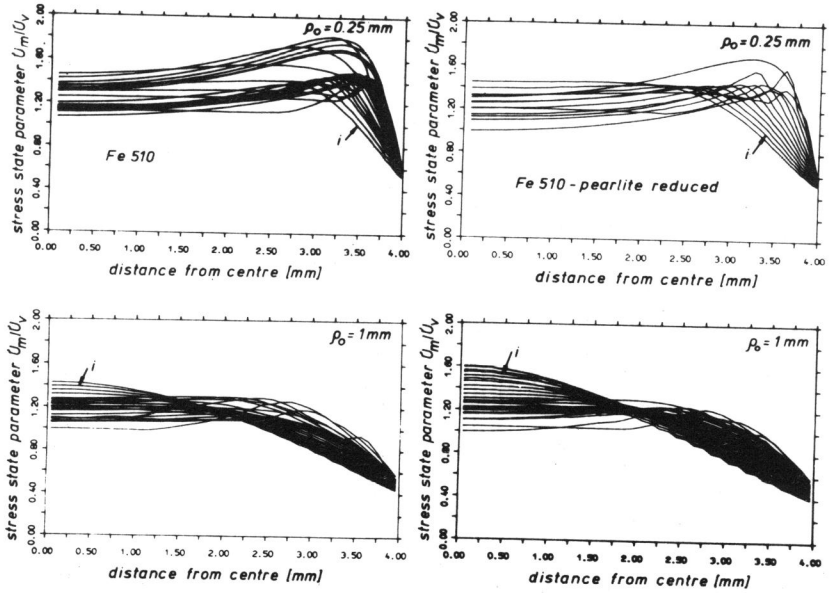

Figure 4 stress state parameters, calculated

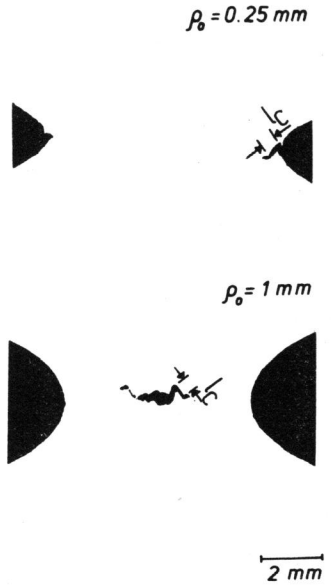

Figure 5 notched specimens

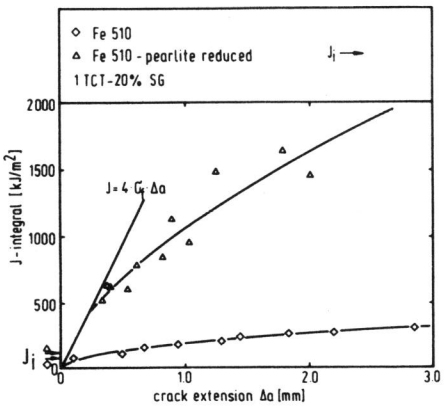

Figure 7 R-curves

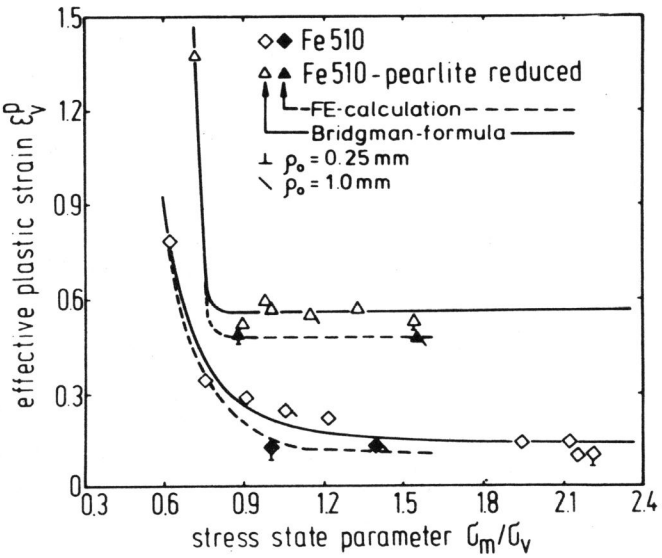

Figure 6 effective plastic strain vs. stress state